Materials Science in Semiconductor Processing 15 (2012) 32–36

Contents lists available at ScienceDirect

Materials Science in Semiconductor Processing

journal homepage: www.elsevier.com/locate/mssp

The influence of thickness and ammonia flow rate on the properties of AlN layers

S. Çörekçi [a,*], M.K. Öztürk [b], M. Çakmak [b], S. Özçelik [b], E. Özbay [c]

[a] Department of Physics, Faculty of Science and Arts, Kırklareli University, 39160 Kırklareli, Turkey
[b] Department of Physics, Faculty of Science and Arts, Gazi University, Teknikokullar, 06500 Ankara, Turkey
[c] Nanotechnology Research Center, Department of Physics, Department of Electrical and Electronics Engineering, Bilkent University, 06800 Ankara, Turkey

ARTICLE INFO

Available online 18 July 2011

Keywords:
AlN thin films
Ammonia flow rate

ABSTRACT

Undoped AlN layers have been grown on *c*-plane sapphire substrates by metal-organic chemical vapor deposition in order to study the effects of ammonia (NH_3) flow rate and layer thickness on the structural quality and surface morphology of AlN layers by high-resolution X-ray diffraction, scanning electron microscopy, and atomic force microscopy. Lower NH_3 flow rate improves crystallinity of the symmetric (0 0 0 2) plane in AlN layers. Ammonia flow rate is also correlated with surface quality; pit-free and smooth AlN surfaces have been obtained at a flow rate of 70 standard cm^3 per minute. Thicker AlN films improve the crystallinity of the asymmetric (1 0 $\bar{1}$ 2) plane.

1. Introduction

A high-quality aluminum nitride (AlN) layer is strongly desired in UV devices due to its wide band gap [1] and in GaN-based transistor structures as a buffer layer [2,3]. Sapphire is one of the most popular substrates for AlN epitaxy because of its wide availability, low cost, and stability at high temperatures. Unfortunately, large lattice and thermal mismatches between AlN and sapphire lead to high dislocation densities in the epitaxial layers. On the other hand, the parasitic reactions between group-13 and group-15 precursors (also referred to as III and V), and the insufficient mobility of Al atoms are serious problems that need to be overcome for high-quality AlN growth, which deteriorate the structural and morphological quality of layers [4,5]. Therefore, researches have primarily focused on the growth of layers with an excellent crystalline quality and a smooth surface by various growth-techniques, -processes, and -parameters. It was reported that the good-quality AlN layers on sapphire substrates are achieved by growth mode modification [6], pulsed atomic-layer epitaxy [7], and thick-layer growth [8]. Okada et al. [1] expressed that thick-layer growth was found to be less effective in improving the crystalline quality of AlN layers. Lobanova et al. [5] showed that flat surfaces are obtained at high temperature, a reduced growth rate, and an optimal V/III ratio. Recently, Banal et al. [9] investigated the effect of the growth parameters for AlN directly grown on sapphire substrates by modified migration-enhanced epitaxy. They observed that the AlN layer has a smooth surface at an optimal growth temperature of 1200 °C, while it has rough surfaces below and above 1200 °C. Hence, the proper selection of growth parameters for achieving a high-quality AlN layer on sapphire substrate is still rather challenging.

In the present study, we have investigated the structure and morphology of the AlN layers grown at different thicknesses and ammonia (NH_3) flows and found that the NH_3 flow rate and the layer thickness have a strong impact on the crystalline quality and surface morphology of the AlN layers.

2. Experimental Details

All the samples were grown on [0 0 0 1]-oriented (*c*-plane) sapphire substrates by low-pressure metal-organic

* Corresponding author.
E-mail address: scorekci@kirklareli.edu.tr (S. Çörekçi).

1369-8001/$ - see front matter © 2011 Elsevier Ltd. All rights reserved.
doi:10.1016/j.mssp.2011.06.003

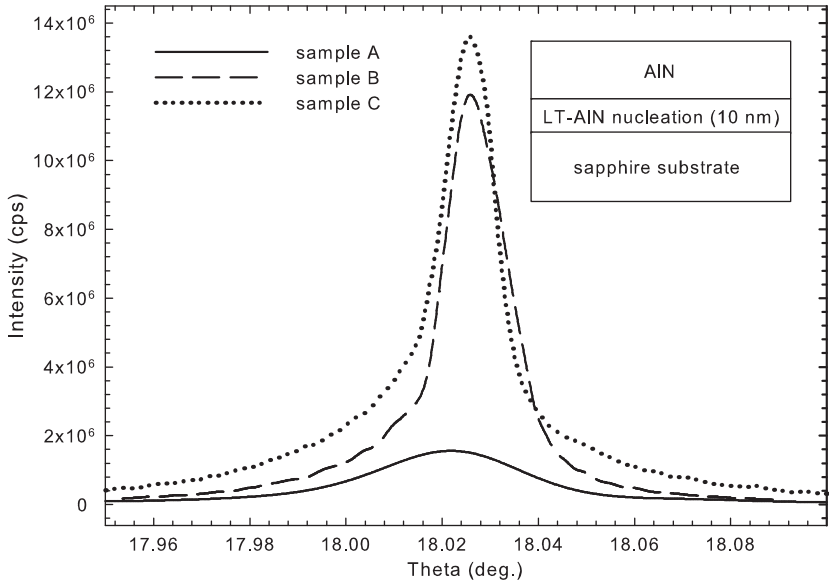

Fig. 1. Symmetric AlN (0 0 0 2) X-ray reflections. The inset shows the schematic sample structure.

Table 1
Structural and morphological parameters of the samples.

	Sample A	Sample B	Sample C
Thickness (nm)	340	550	750
NH_3 (sccm)	125	70	70
Screw-type TD density (cm^{-2})	3.5×10^{7}	6.4×10^{6}	5.5×10^{6}
Edge-type TD density (cm^{-2})	8.1×10^{10}	3.9×10^{11}	2.0×10^{11}
Tilt angle (°)	0.0026	0.0008	0.0011
Lateral coherence length (nm)	1130	4500	2250
a-lattice constant (nm)	0.31004	0.32379	0.30768
c-lattice constant (nm)	0.49609	0.48614	0.48790
In-plane strain (ε_a)	−0.00354	0.04066	−0.01112
Out-of-plane strain (ε_c)	−0.00368	−0.02366	−0.02012
Surface rms roughness (nm)	0.11	0.06	0.10
Surface pit density (cm^{-2})	3.5×10^{8}	–	–

chemical vapor deposition (MOCVD). Trimethylaluminum (TMAl) and NH_3 were used as sources for Al and N, respectively, in which hydrogen (H_2) was used as the carrier gas. The structure of the samples is shown schematically in the inset of Fig. 1. Before the growth of AlN, sapphire substrates were annealed at 1080 °C for 10 min to remove surface contamination. In all of the samples, a 10 nm-thick AlN NL was first deposited at a reactor pressure of 50 mbar and a growth temperature of 840 °C. Then, the reactor temperature was ramped to 1140 °C and an AlN main layer was grown at a reactor pressure of 25 mbar and a growth temperature of 1140 °C. The nitridation, nucleation, and annealing processes of the samples were performed at the same conditions. As is seen in Table 1, AlN-samples having thicknesses of 340, 550, and 750 nm are grown at 125, 70, 70 standard cm^3 per minute (sccm) NH_3 flow rates were labeled as samples A, B, and C, respectively.

The samples were characterized by high-resolution X-ray diffraction (HRXRD), scanning electron microscopy (SEM), and atomic force microscopy (AFM) measurements. HRXRD measurements were performed by a Bruker D8-Discover high-resolution diffractometer by $CuK_{\alpha1}$ radiation, a prodded mirror, and a 4-bounce Ge (0 2 2) monochromator. AFM scans were carried out at room temperature by Omicron variable temperature (VT) STM/AFM, and the images were collected at $2\times2\ \mu m^2$ scale. The root-mean-square (rms) roughnesses of the samples were processed from their surface topographies with Scala Pro software. The SEM surface micrographs were taken using a JEOL JSM-6060LV SEM instrument.

3. Results and discussion

Fig. 1 shows the X-ray ω-scans (so-called the rocking curves) that were obtained from the symmetric (0 0 0 2) plane of the AlN layers in the samples. AlN (0 0 0 2) reflections for all the samples were observed at different diffraction angles. The shift in the peak positions of the samples can be related to the strained nature of the layers. In addition, the intensities of the peaks are proportional to thicknesses of the layers. From the ω-scans, the (0 0 0 2) full-width at half-maximums (FWHMs) of the AlN (0 0 0 2) reflections for samples A, B, and C were determined as 126, 54, and 50 arcsec, respectively. There is no major difference in the FWHM values of samples B and C, and these values are similar to or slightly better than those of previously reported AlN epifilms [1,10]. Furthermore, the AlN (0 0 0 2) reflections of samples B and C are significantly narrower than that of sample A. This result clearly shows that reducing the NH_3 flow rate improves the crystalline quality of the symmetric (0 0 0 2) plane. This is in agreement with the findings of Thapa et al. [4] who investigated the effects of V–III ratio, N_2–H_2 ratio, and growth temperature on the structural properties of AlN layers grown on *c*-plane sapphire substrates, and found that the low V/III ratio is an eminent growth condition for crystallographic perfection due to the

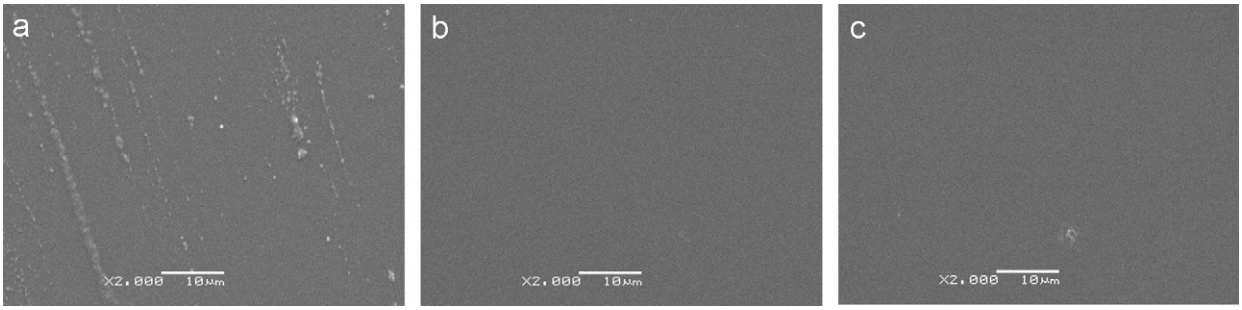

Fig. 2. Plain-view SEM micrographs of samples: (a) A, (b) B, and (c) C.

minimized parasitic reactions between the precursors in the gas phase during growth. On the other hand, the (1 0 $\bar{1}$ 2) FWHMs of samples A, B, and C were obtained as 3812, 8359, and 6005 arcsec, respectively. The asymmetric (1 0 $\bar{1}$ 2) reflections of samples B and C have the larger FWHM values, and these values increase by reducing the NH_3 flow rate, as opposed to the (0 0 0 2) reflections. The (1 0 $\bar{1}$ 2) FWHM of sample C is slightly better than that of sample B. This result shows that increasing the thickness of the layer is effective in improving the crystalline quality of the asymmetric (1 0 $\bar{1}$ 2) plane in AlN layers rather than the symmetric one, (0 0 0 2).

The broadening of X-ray diffraction (XRD) peaks is mainly due to the limited crystallite size, misorientation of crystallites, and microstrain in epitaxial layers [11,12]. Additionally, the out-of-plane and in-plane misorientations of crystallites in the layers are related to the screw and edge threading dislocations (TDs), respectively [11]. The screw and edge TD densities of AlN in the samples can be calculated from the following equations [13]:

$$D_S = \frac{\beta^2_{(0002)}}{4.35|b_S|^2},\ D_E = \frac{\beta^2_{(10\bar{1}2)}}{4.35|b_E|^2} \quad (1)$$

where D_S is the screw dislocation density, D_E is the edge dislocation density, β is the FWHM value of the AlN (0 0 0 2) and AlN (10$\bar{1}$2) reflections, and $|b|$ is the Burgers vector length of the dislocation ($|b_S|=0.49792$ nm, $|b_E|=0.31114$ nm). The screw and edge TD densities were obtained respectively as 3.5×10^7 and 8.1×10^{10} cm^{-2} for sample A, 6.4×10^6 and 3.9×10^{11} cm^{-2} for sample B, and 5.5×10^6 and 2.0×10^{11} cm^{-2} for sample C. In all of the samples, the screw dislocation density is quite low than the edge one, which is typical for AlN thin films. On the other hand, it is clear that the dislocation density decreases with increasing layer thickness for AlN grown at the same NH_3 flow rate in samples B and C. In case of increasing thickness and decreasing NH_3 flow rate from sample A to sample B (or sample C), the increase in edge-type TD density of AlN can be attributed to the decrease in the NH_3 flow rate because the increase in thickness has the opposite effect as seen from the behaviors of samples B and C.

We used the mosaic model to evaluate, in detail, the structural quality of the AlN layers in the samples. It is well known that epitaxial films with high dislocation density are often described by the mosaic model [14]. In this model, a mosaic layer consists of single crystalline blocks with lateral and vertical coherence lengths. As was previously mentioned, XRD peaks are broadened due to the out-of-plane and in-plane rotation of the blocks (tilt and twist), limited crystallite size, and microstrain [11,12]. Detailed knowledge about this model can be obtained from Ref. [14]. In the present work, we have primarily focused on the relation between the structural and morphological properties of the AlN layers in the samples. Thus, the tilt angles and lateral coherence lengths of the AlN layers have been determined from the mosaic model, and the results were tabulated in Table 1. The tilt angles of the AlN layers in samples A, B, and C were 0.0026°, 0.0008°, and 0.0011° and the lateral coherence lengths were as 1130, 4500, and 2250 nm, respectively. From the results that were obtained by mosaic model, it is clearly seen that the quality of the symmetric (0 0 0 2) plane in samples B and C are better than that of sample A, and these results are in good agreement with (0 0 0 2) FWHMs of the ω-scans.

We have also calculated the lattice parameters of the AlN layers in the samples using Bragg's Law and the hexagonal crystallographic formula, and evaluated strain state of the layers. The relaxed (unstrained) in-plane (a)- and out-of-plane (c)-lattice constants have been taken as 0.31114 and 0.49792 nm for AlN. The a- and c-lattice constants of the AlN layers were obtained as 0.31004 and 0.49609 nm for sample A, 0.32379 and 0.48614 nm for sample B, and 0.30768 and 0.48790 nm for sample C. From the lattice constants, the in-plane (ε_a) and out-of-plane (ε_c) strain values of the layers were calculated as −0.00354 and −0.00368 for sample A, 0.04066 and −0.02366 for sample B, and −0.01112 and −0.02012 for sample C. It can be seen that the in-plane and out-of-plane strains for all of the AlN layers are compressive (negative strain) type except for the in-plane strain of the AlN layer in sample B, which is the tensile (positive strain) type. Moreover, the strain values of sample A are one order of magnitude lower than those of samples B and C. This result might be related to the stoichiometry of the AlN layers in the samples or density of point defects in the layers.

Fig. 2 shows a set of plain-view SEM micrographs of the samples. Compared to the hillock-like surface of sample A, samples B and C displayed mirror-like surfaces in a large region. No cracks were observed in the micrographs of the samples. To further understand the surface

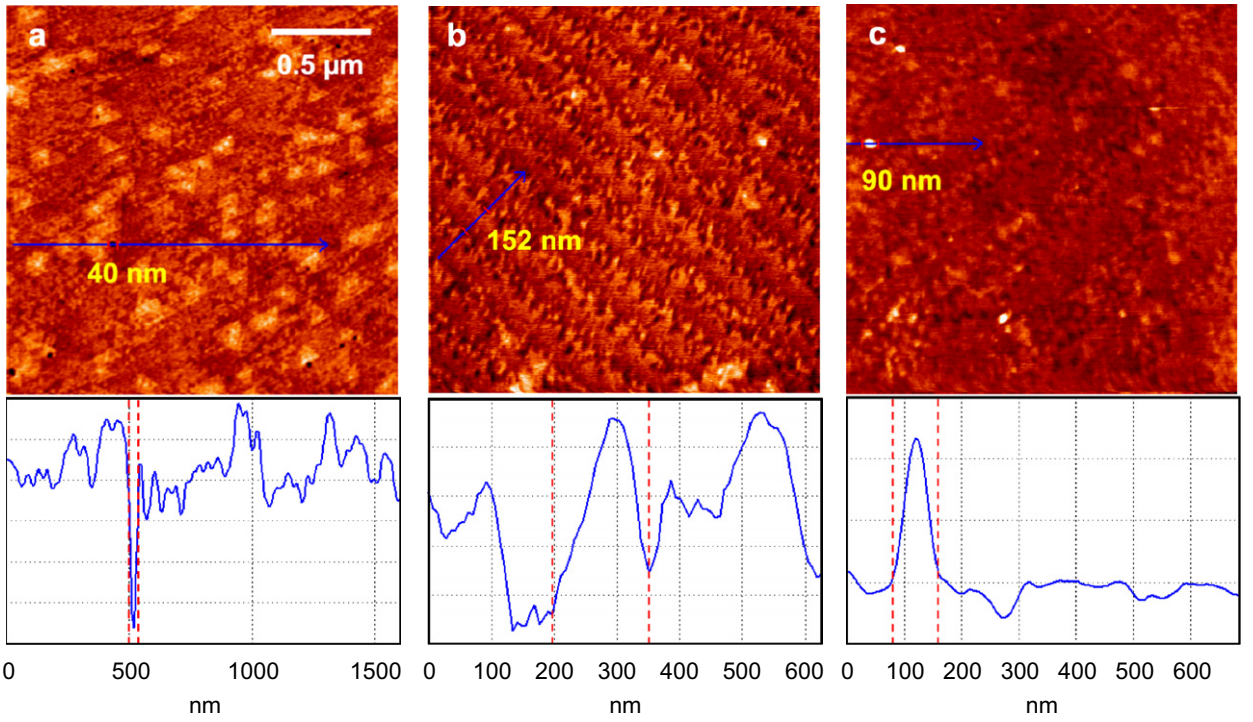

Fig. 3. AFM images of samples: (a) A, (b) B, and (c) C. The scan areas are $2 \times 2\ \mu m^2$.

properties of the samples, AFM measurements were carried out in a narrow area on the as-grown samples. Fig. 3 shows AFM images with a $2 \times 2\ \mu m^2$ scan area of the samples. There appeared dark pits of varying size and diameter on the surface of sample A and they traveled deep into the AlN epitaxial layers (Fig. 3a). The average pit diameter was determined as 40 nm from the AFM line profile as seen in Fig. 3a. The pit density was estimated as $3.5 \times 10^8\ cm^{-2}$ by the number of pits in the AFM image. Similarly, Gherasimova et al. [15] reported the appearance of V-shaped grooves with varying width and depth on the AlN surface at increased NH_3 flow rate. In the same way, Banal et al. [9] observed the pits on AlN samples grown by MOCVD. In their study, the pit formation was attributed to a greater amount of the group V, since NH_3 decomposition under a high V/III ratio provided the active N species more than what is necessary for AlN growth. In addition, the 3D character of the morphology implies a limited Al adatom diffusion in N-rich conditions [15,16]. On the other hand, Liu et al. [17] reported that strain energy and the reduction of surface mobility are major attributors in the pit formation. Within this framework, the pitted morphology of sample A is probably from the excess N species, strain, and the low surface mobility due to relatively high ammonia flow rate.

Contrary to sample A, samples B and C are grown at low NH_3 flow rate exhibited pit-free surfaces (Fig. 3b, c). At the same time, sample B had step-flow morphology consisting of an array of step-terrace. As is known, the step-flow growth enables a smooth surface and is important for device performance [18]. The terrace width on the surface of sample B was approximately measured as 152 nm by the AFM line profile. The large lateral terrace size (>100 nm) implies a low surface roughness [18], which is in good agreement with our previous reports [3,19]. The rms parameter is commonly used to evaluate surface roughness of epitaxial thin films. The rms roughnesses of samples A, B, and C were measured as 0.11, 0.06, and 0.10 nm over a $2 \times 2\ \mu m^2$ scan area as listed in Table 1. According to the rms values, three of the samples have flat surfaces. However, the pits and hillocks in the AFM and SEM images of sample A reveal that it has a rough surface. This discrepancy in the rms value of sample A is probably originated from the small probed area of AFM.

Among the present samples, sample A has the lowest lateral coherence length, the largest tilt angle, and the highest (0 0 0 2) FWHM value as listed in Table 1, which are consistent with the SEM and AFM results. These results clearly demonstrate that sample A has the poorest surface quality. Its imperfect surface is related to the smaller diffusion length of Al atoms because of relatively high NH_3 flow rate. Contrary to sample A, samples B and C grown at low NH_3 flow rates have pit-free and smooth surfaces. Furthermore, the large lateral coherence length and low tilt angle of sample B confirm that step-flow growth leads an atomically flat surface. Consequently, the high-quality of the (0 0 0 2) plane for both samples, which was revealed in the XRD measurements, is accompanied by improving the surface quality. The enhanced diffusion lengths of the Al atoms due to the low NH_3 flow and the reduced parasitic reactions between the TMAl and NH_3 precursors owing to the low V/III ratio are the likely reasons for this improvement.

4. Conclusion

AlN films have been grown on *c*-plane sapphire substrates by MOCVD. The effects of the NH_3 flow rate and film thickness on the structure and morphology of AlN have been investigated by HRXRD, SEM, and AFM measurements. The HRXRD results clearly show that the low NH_3 flow rate improves the crystalline quality of the symmetric (0 0 0 2) plane in the films. Also, it has been determined that the layer thickness is effective in improving the quality of asymmetric (1 0 $\bar{1}$ 2) plane. The SEM and AFM measurements show that the surface quality is rather sensitive to NH_3 flow rate. Pits have been observed on the film grown at NH_3 flow rate of 125 sccm. However, the pitted morphology has not been observed at the relatively low NH_3 flow rate of 70 sccm, in which the AlN films exhibited atomically flat and pit-free surfaces.

Acknowledgments

This work has been supported by the Turkish State Planning Organization, project number 2011K120290, and the Scientific and Technological Research Council of Turkey. One of the authors (E. O.) also acknowledges partial support from the Turkish Academy of Sciences.

References

[1] N. Okada, N. Kato, S. Sato, T. Sumii, T. Nagai, N. Fujimoto, et al., Journal of Crystal Growth 298 (2007) 349.
[2] M. Miyoshi, H. Ishikawa, T. Egawa, K. Asai, M. Mouri, T. Shibita, et al., Applied Physics Letters 85 (2004) 1710.
[3] S. Çörekçi, M.K. Öztürk, B. Akaoğlu, M. Çakmak, S. Özçelik, E. Özbay, Journal of Applied Physics 101 (2007) 123502.
[4] S.B. Thapa, C. Kirchner, F. Scholz, G.M. Prinz, T. Thonke, R. Sauer, et al., Journal of Crystal Growth 298 (2007) 383.
[5] A.V. Lobanova, E.V. Yakovlev, R.A. Talalaev, S.B. Thapa, F. Scholz, Journal of Crystal Growth 310 (2008) 4935.
[6] J. Bai, M. Dudleya, W.H. Sun, H.M. Wang, M. Asif Khan, Applied Physics Letters 88 (2006) 051903.
[7] J.P. Zhang, M.A. Khan, W.H. Sun, H.M. Wang, C.Q. Chen, Q. Fareed, et al., Applied Physics Letters 81 (2002) 4392.
[8] M. Imura, K. Nakano, T. Kitano, N. Fujimoto, N. Okada, K. Balakrishnan, et al., Physica Status Solidi A 203 (2006) 1626.
[9] R.G. Banal, M. Funato, Y. Kawakami, Journal of Crystal Growth 311 (2009) 2834.
[10] J. Bai, T. Wang, P. Comming, P.J. Parbrook, J.P.R. David, A.G. Cullis, Journal of Applied Physics 99 (2006) 023513.
[11] H. Jiang, T. Egawa, M. Hao, Y. Liu, Applied Physics Letters 87 (2005) 241911.
[12] M.E. Vickers, M.J. Kappers, R. Datta, C. McAleese, T.M. Smeeton, F.D.G. Rayment, et al., Journal of Physics D: Applied Physics 38 (2005) A99.
[13] C.G. Dunn, E.F. Koch, Acta Metallurgica 5 (1957) 548.
[14] R. Chierchia, T. Böttcher, H. Heinke, S. Einfeldt, S. Figge, D. Hommel, Journal of Applied Physics 93 (2003) 8918.
[15] M. Gherasimova, G. Cui, Z. Ren, J. Su, X.L. Wang, J. Han, et al., Journal of Applied Physics 95 (2004) 2921–2923.
[16] F. Widman, B. Daudin, G. Geuillet, N. Pelekanos, J.L. Rouviere, Applied Physics Letters 73 (1998) 2642.
[17] J.P. Liu, B.S. Zhang, M. Wu, D.B. Li, J.C. Zhang, R.Q. Jin, et al., Journal of Crystal Growth 260 (2004) 388–393.
[18] A. Torabi, P. Ericson, E.J. Yarrantom, W.E. Hooke, Journal of Vaccine Science Technology B 20 (2002) 1234.
[19] S. Çörekçi, M.K. Öztürk, A. Bengi, M. Çakmak, S. Özçelik, E. Özbay, Journal of Materials Science 46 (2011) 1606–1612.